^{144}Sm(p,p') scattering through isobaric analog resonances and the structure of ^{145}Sm

M. L. Cescato and M. C. Hermida M. Ruiz
Instituto de Física, Universidade de São Paulo, São Paulo, Brasil

J. L. Foster, Jr.
Department of Physics, University of Notre Dame, Notre Dame, Indiana 46556 and Intermetrics, Inc., Warminster, Pennsylvania 19044

F. Krmpotić*
Instituto de Física, Universidade de São Paulo, São Paulo, Brasil and Departamento de Física, Facultad de Ciencias Exactas, Universidad Nacional de La Plata, 1900 La Plata, Argentina

(Received 14 September 1982)

Angular distributions of the cross section for the elastic and inelastic scattering of protons have been measured at four isobaric analog resonances of the ^{144}Sm+p system and at two off-resonance energies. Spectroscopic information about the $\frac{7}{2}^-_1$, $\frac{3}{2}^-_1$, $\frac{1}{2}^-_1$, and $\frac{5}{2}^-_1$ states of the parent nucleus ^{145}Sm is extracted, with the core ^{144}Sm in the states 0^+_1, 2^+_1, 3^-_1, 4^+_1, and 2^+_2. The analysis includes direct and fluctuating nonresonant processes. The direct scattering amplitude is obtained from a coupled channel treatment. Different methods for the calculations of the single-particle widths have been employed. The experimental spectroscopic amplitudes were compared with nuclear structure calculations based on the particle-vibrator model. Both the liquid drop model and the quasiparticle random phase approximation were used to describe the vibrator. The calculations based on the latter model show good agreement with the experimental results.

[NUCLEAR REACTIONS ^{144}Sm(p,p'), $E=8.5-14$ MeV, enriched targets, measured $\sigma(E_p,\theta)$; experimental and theoretical ^{145}Sm spectroscopic amplitudes.]

I. INTRODUCTION

Several experimental studies of the isobaric analog resonances in the ^{144}Sm+p system (^{145}Eu) have been reported[1-4] so far. In these works information about energies, widths, spins, and parities of the resonances, associated with the low-lying states of the parent nucleus ^{145}Sm, were obtained through the analysis of elastic excitation functions. A few works appear in the literature on inelastic decays, namely, several highly excited particle-hole states in ^{144}Sm were studied by Martin *et al.*,[3] while the decay to the first excited 2^+ states was analyzed by Clement *et al.*[4] employing the DWBA prescription to account for the nonresonant scattering.

In the present work we analyze the elastic and inelastic decays of the isobaric analog resonances in the ^{144}Sm+p system associated with four low-lying states of the parent nucleus ^{145}Sm. We consider the inelastic decays to the 2^+_1, 3^-_1, 4^+_1, and 2^+_2 states of ^{144}Sm, as the experimental data reported by Martin *et al.*[3] clearly indicate that all of them play an important role in building up the wave functions of the considered parent nucleus states. We make use of the coupled channel formalism for treating the direct nonresonant scattering. In addition, we also include the fluctuating nonresonant contributions to the cross section (Hauser-Feshbach). This effect is usally ignored since the fluctuating decay occurs preferentially through the open neutron channel, turning negligible the fluctuating contribution in the proton channel. This, however, is not the case for the first two isobaric resonances in the ^{144}Sm+p system, since they lie near the neutron threshold.

The determination of spectroscopic amplitudes involves theoretical estimates for single-particle resonance amplitudes (g^{sp}), and it was established by Harney and Weidenmüller[5] that the results may vary appreciably depending on the approach employed in treating the absorption in the $T^<$ states. In the present work we calculated the single particle resonance amplitudes using four different approaches.[6-10] The application of sum rules to the spectroscopic amplitudes resulting from the various approaches for g^{sp} provides us a check on the reliability of the various methods, along with a test of consistency for the experimental spectroscopic amplitudes.

Theoretical predictions for the spectroscopic amplitudes are obtained in the framework of the particle-vibrator model and compared to the experimental values. The vibrator is described at first by a liquid drop model and later treated within the quasiparticle random phase approximation (QRPA).

II. EXPERIMENT

The experiment was performed at the Universidade de São Paulo Pelletron-8UD accelerator laboratory. Angular distributions of the elastic and inelastic cross sections of protons scattered by ^{144}Sm were measured at beam ener-

 ©1984 The American Physical Society

TABLE I. Optical model parameters. The real potential depth is given by $V=V_0-\kappa E_p$ MeV, where E_p is the incident particle energy in the laboratory frame.

V_0 (MeV)	κ	R_R (fm)	a_R (fm)	W_S (MeV)	R_S (fm)	a_S (fm)	V_{so} (MeV)	R_{so} (fm)	a_{so} (fm)	R_C (fm)
59.60	0.55	6.552	0.7113	9.02	6.709	0.6703	6.2	5.766	0.7113	6.290

gies of 9.315, 10.205, 10.905, and 10.985 MeV. These values are equal to or very close to the energies of the first $\frac{7}{2}^-$, $\frac{3}{2}^-$, $\frac{1}{2}^-$, and $\frac{5}{2}^-$ analog resonances in the ^{144}Sm+p system. The $\frac{7}{2}^-$ resonance was located by looking for the maximum yield of the protons leaving ^{144}Sm in the neutron particle-hole states.[3] The angular distributions were measured in 10° steps from $\theta_{lab}=40°$ to 169°. In order to obtain information about the nonresonant background, additional angular distributions were observed at 8.50 and 14.00 MeV in the intervals $\theta_{lab}=30°$ to 160° and 40° to 169°, respectively, in steps of 10°. At these energies contributions from resonant scattering vanish.

The detection system consisted of three surface barrier detectors, positioned 10° apart, each of which subtended a solid angle of about 1 msr. The resolution of the detectors was improved by water cooling them to 0° C.

The targets were prepared by vacuum evaporation of 86% enriched ^{144}Sm, from a mixture of Sm_2O_3 and La, allowing the simultaneous evaporation of Sm and reduction of La to La_2O_3. The target thicknesses were of nominally 300 and 200 μg/cm^2. The thicker targets were used for the measurements at 14.00 MeV, thus maintaining the energy loss in the target at about 5 keV for all bombarding energies. The overall energy resolution was about 25 keV. The absolute cross-section normalization, accurate to about 5%, was determined from the elastic scattering data by comparison to optical model cross-section calculations at forward angles, where the optical model is a small correction to Rutherford scattering. The error bars on the data points indicate only statistical errors.

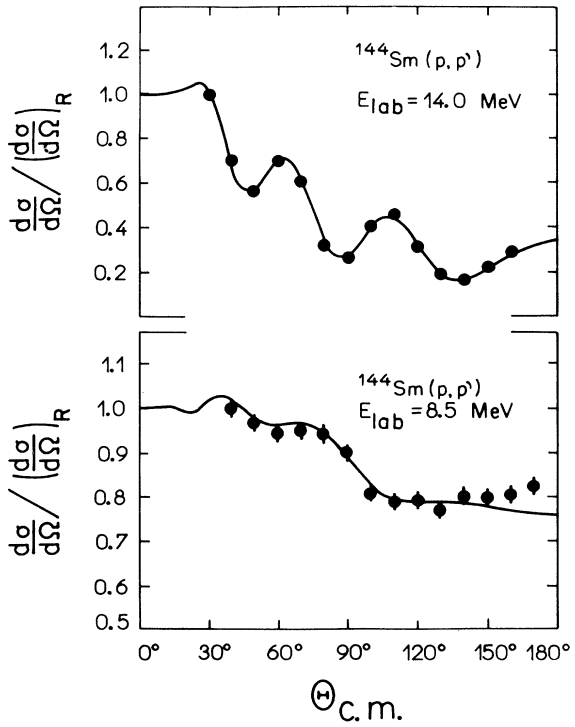

FIG. 1. Elastic angular distributions at 8.5 and 14.0 MeV.

The form of the optical potential is

$$U(r)=V_C-Vf(r,R_N,a_N)-iW_S\frac{d}{dr}f(r,R_S,a_S)$$
$$+V_{so}(\vec{\sigma}\cdot\vec{l})\left[\frac{\hbar}{m_\pi c}\right]^2\frac{1}{r}\frac{d}{dr}f(r,R_{so},a_{so}),$$

where $f(r,R,a)$ is the usual Saxon-Woods form. The parametrization corresponding to the fits is presented in Table I.

III. ANALYSIS OF THE EXPERIMENTAL DATA

The analysis consisted of two parts. First the nonresonant (background) scattering was studied at off-resonance energies and was then used as a basis to extract an interpolated background in the analysis of the resonance.

The data at 8.5 and 14.0 MeV allowed the analysis of the nonresonant scattering. From the elastic scattering we determined the optical potential parameters and their energy dependence. These parameters were also tested in the analysis of the inelastic scattering data. In addition, "best values" for the deformation parameters involved in the description of the direct inelastic scattering were obtained from the literature. Since at 8.5 MeV few neutron channels are open for the compound nucleus decay, a significant contribution in the proton channels is present (neutron threshold ~7 MeV).

Fits of the elastic angular distributions at 14.0 and 8.5 MeV, using the optical potential parameters listed in Table I, are shown in Fig. 1. Initial values for the optical parameters were obtained from Refs. 3 and 11, and the fits were done using the optical model code MAGALI.[12] The measured back-angle cross sections at 8.5 MeV are somewhat higher than the shape elastic prediction, since fluctuating processes are contributing. Such processes should be even more pronounced in the inelastic cross sections. With the assumption of a linear energy dependence for the real potential depth V, we obtained the relation

$$V=-0.55E_p+59.6 \text{ MeV},$$

where E_p is the incident particle energy in the laboratory frame. The surface imaginary potential depth W_S was assumed to be independent of the energy.

The inelastic background comes from both direct and fluctuating processes. The direct inelastic scattering can be described as resulting from the excitation of the surface

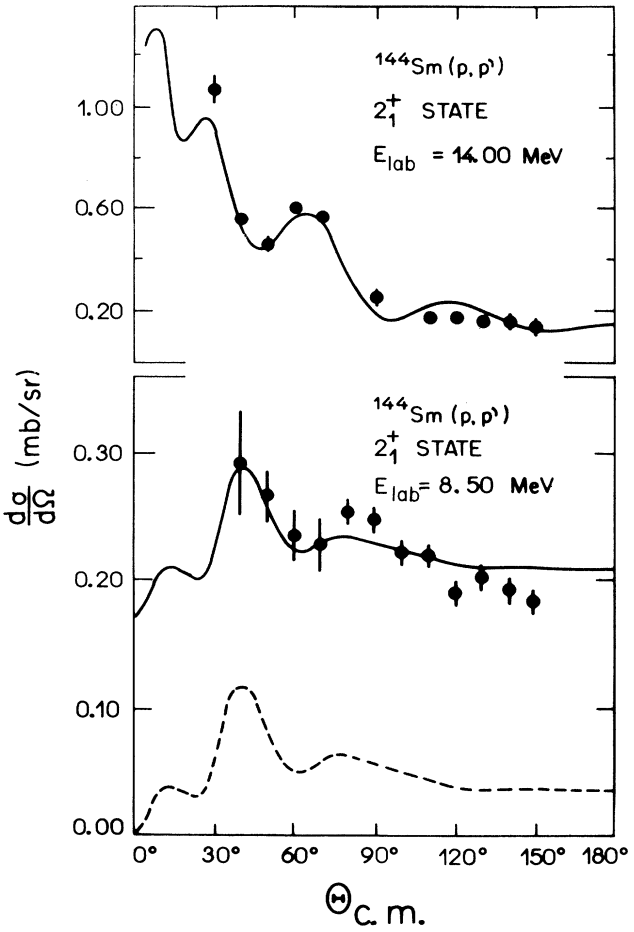

FIG. 2. Inelastic angular distribution of the cross section for the 2_1^+ state at 8.5 and 14.0 MeV. The solid curves correspond to the total cross section. At 14.0 MeV only direct processes contribute and the curve corresponds to the coupled channel calculation with $\delta_2=0.46$ fm. At 8.5 MeV the solid curve results from adding the direct contribution calculated in the same way (dashed line) to the fitted compound nucleus contribution (0.17 mb/sr).

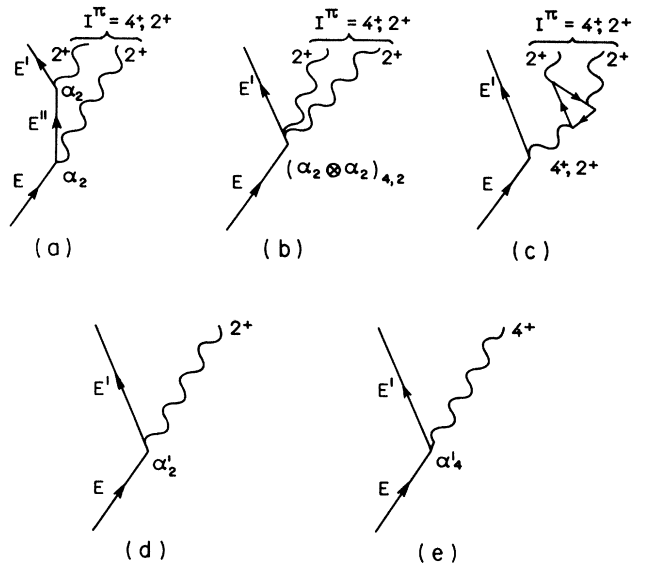

FIG. 3. Graphical representation of the excitation mechanism for the 2_2^+ and 4_1^+ two-quadrupole phonon states. Within model I, which does not include the anharmonic effects, the 2_2^+ and 4_1^+ states are attained only via two-step processes shown in graph (a). However, when one considers also the contributions from the second derivative of the optical potential, the term gives rise to the excitations sketched in graph (b). Diagram (c) shows the excitation of the two-quadrupole phonon states through the anharmonic effects induced by the particle-phonon coupling. This type of excitation of the 2_2^+ and 4_1^+ states can be simulated by effective $\lambda=2$ and $\lambda=4$ vibrational fields as illustrated in graphs (d) and (e), respectively.

vibrational modes of the spherical target nucleus ^{144}Sm. This kind of scattering is essentially characterized by the deformation lengths

$$\delta_\lambda=\beta_\lambda R \ ,$$

where β_λ is the deformation parameter for the vibrational mode λ. For each radius of the optical potential (Coulomb R_C, real volume R_N, surface imaginary R_S) a corresponding deformation parameter (β_λ^C, β_λ^N, β_λ^S) is defined, such that

$$\delta_\lambda=\beta_\lambda^N R_N=\beta_\lambda^C R_C=\beta_\lambda^S R_S \ .$$

The deformation lengths are already available in the literature from analyses of inelastic angular distributions at several energies.[13–16] For the 2_1^+ state several δ_2 values, which differ significantly with each other, have been reported. Comparison between the experimental inelastic angular distribution at 14 MeV and coupled channels calculations using the ECIS code[17] showed that the best agreement is achieved with the δ value of Larson *et al.* ($\delta_2=0.46$ fm).[16] The result for this value of δ_2 is illustrated in Fig. 2.

Figure 2 also shows the 8.5 MeV experimental inelastic angular distribution compared to that calculated for $\delta_2=0.46$ fm. Here the fluctuation contribution accounts for most of the cross section. At this energy only the neutron and proton channels are significant for compound nucleus decay. A Hauser-Feshbach (HF) calculation for proton decay of the compound nucleus involves the ^{144}Sm and ^{144}Eu optical potentials and the levels and level density parameters of these same nuclei. Level density estimates are always uncertain, and information on the low lying states of ^{144}Eu, on which a HF calculation critically depends, is sparse. As a consequence, the predictions of HF calculations in our work are reliable only in order of magnitude, and the HF contribution was taken as an additive isotropic cross section to be treated as a fitting parameter in the inelastic scattering analysis. The validity of this rests on the isotropy of the HF contribution in the proton channel. For protons the combined centrifugal and Coulomb barriers drastically inhibit the partial waves with $l\neq 0$. Taking $\sigma^{fl}\simeq 0.17$ mb/sr nicely fits the 8.5 MeV inelastic data, as is shown in Fig. 2.

The 4_1^+ and 2_2^+ states may be interpreted as being built up from two harmonic quadrupole phonons. This description is illustrated in Figs. 3(a) and (b), and has been

TABLE II. Deformation lengths for ^{144}Sm states. The δ_λ values are taken from Ref. 16.

I_n^π	E_{exc} (MeV)	λ	δ_λ (fm)
2_1^+	1.661	2	0.46
3_1^-	1.811	3	0.87
4_1^+	2.191	4	0.33
2_2^+	2.423	2	0.29

used in a coupled channels calculation (ECIS), with $\delta_2=0.46$ fm, at 30 MeV, since at this energy it is possible to compare the results with the data of Larson *et al.*[16] The calculated cross sections were about 50 times smaller than the measured ones. This fact indicates that the anharmonic effects [shown in Fig. 3(c)], which are not included in the coupled channels calculation, should play an important role. These effects can be taken into account by introducing new "effective" deformation parameters β_4' and β_2' and treating the 4_1^+ and 2_2^+ states as one phonon excitations, corresponding to the new effective amplitudes [see Figs. 3(d) and (e)]. Within this approach, which was adopted throughout this work, the experimental data were well described. The deformation lengths for all the studied states are presented in Table II.

Neglecting the fluctuating contribution to the cross section, the scattering at the resonances energies is described through the scattering matrix

$$S_{cc'}=S_{cc'}^{\rm dir}-e^{i(\phi_c+\phi_{c'})}\sum_\nu \frac{g(J_\nu,c)g(J_\nu,c')}{E-E_{J_\nu}+\frac{i}{2}\Gamma_{J_\nu}}\ , \tag{3.1}$$

where $c\equiv\{l,j,I\}$, with $\{l,j\}$ the orbital and total angular momenta of the incident proton and I the spin of the target; J_ν is the spin of the νth resonance; $\phi_c=\xi_c+\sigma_c+\psi_c^R$, where ξ_c is the real optical model phase shift, σ_c^R the Coulomb phase shift, and ψ_c^R the resonance mixing or asymmetry phase; and E_{J_ν} and Γ_{J_ν} are the energy and total width of the J_ν resonance, respectively. The resonance (or escape) amplitudes $g(J_\nu,c)$ are related to the spectroscopic amplitudes $\theta(c,J_\nu)$ and partial widths $\Gamma_{J_\nu,c}$ through the relations

$$\theta(c,J_\nu)=\frac{g(J_\nu,c)}{g^{\rm sp}(J_\nu,c)} \tag{3.2}$$

and

$$\Gamma_{J_\nu,c}=|g(J_\nu,c)|^2\ , \tag{3.3}$$

where $g^{\rm sp}(J_\nu,c)$ are the single particle amplitudes in channel c at the J_ν resonance energy.

The direct amplitude $S_{cc'}^{\rm dir}$ was determined from the analysis of the off-resonance data presented in the preceding section. The fit of the elastic cross section involves as parameters only the elastic partial width $\Gamma_{J_\nu}^0$, the energy E_{J_ν}, and total width Γ_{J_ν} of the resonance. With these parameters determined from the analysis of elastic scattering, the remaining parameters in the inelastic angular distributions fits were the inelastic partial widths. The fluctuating contribution to the cross section was obtained as a fitted additive parameter to the cross section described by the S matrix.

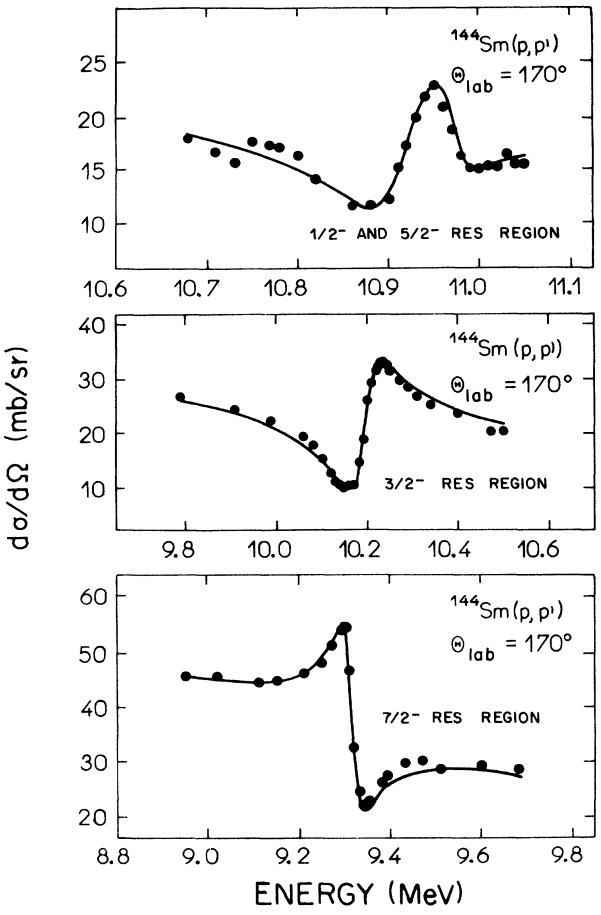

FIG. 4. Fits to 170° elastic excitation function over the four analyzed resonances. The corresponding parametrization is presented in Table III.

The fluctuating contributions to the elastic cross section at the resonance energies were estimated through Hauser-Feshbach calculations using the code CINDY.[18] We have used the level density parameters of Gilbert and Cameron[19] and the optical potential of Becchetti and Greenlees[20] for ^{144}Eu. It turned out that in all cases the elastic fluctuating cross section was of the same order of magnitude as the experimental error, and hence was disregarded.

The elastic scattering at the resonances of interest has been extensively studied. This fact enabled us to employ the resonance parameters available in the literature.[1–4] The best choice of resonance parameters E_{J_ν}, Γ_{J_ν} and elastic partial widths $\Gamma_{J_\nu,c}$ was determined through the reanalysis of the 170° elastic excitation function of Marouchian *et al.*[1] It was also possible to determine the asymmetry phases during this procedure. The code ANSPEC (Ref. 21) was employed in calculating the excitation function. The resulting fits can be seen in Fig. 4 and the corresponding final parametrization is presented in Table III. These same parameters were used to calculate the elastic angular distributions shown with the measured

TABLE III. Resonance parameters and elastic partial widths. The quantity ΔE is defined as the difference between the beam and resonance energies (laboratory frame). The parameters of those resonances marked by an asterisk were taken from Ref. 4 and used in background for the other resonances (see Fig. 4). The $\frac{7}{2}_1^-$ resonance energy (9.251 MeV) is taken from Ref. 3. The energies of the $\frac{3}{2}_1^-$, $\frac{1}{2}_1^-$, and $\frac{5}{2}_1^-$ resonances are relative to 9.251 MeV.

J_ν^π	$E_{\rm res}^{J_\nu}$(c.m.) (MeV)	$\Gamma_T^{J_\nu}$ (keV)	Γ_J^0 (keV)	ψ_l	ΔE (keV)
$\frac{7}{2}_1^-$	9.251	49	7.8	0°	0
$\frac{3}{2}_1^-$	10.135	70	22.0	8°	0
$\frac{9}{2}_1^-$ *	10.690	47	0.7		
$\frac{1}{2}_1^-$	10.835	90	31.5	8°	−5
$\frac{5}{2}_1^-$	10.904	51	4.1	0°	5
$\frac{9}{2}_2^-$ *	11.040	50	0.3		
$\frac{7}{2}_2^-$ *	11.120	36	1.7		
$\frac{3}{2}_2^-$ *	11.220	52	9.7		
$\frac{5}{2}_2^-$ *	11.240	45	6.9		

cross sections in Fig. 5. From these angular distributions a determination was made of the difference

$$\Delta E = E_{J_\nu} - E \ , \tag{3.4}$$

where E is the beam energy during the experiment. The value of ΔE was varied with a 5 keV interval (the uncertainty in localizing the resonances), and the ΔE value which provided the best descriptions of the experimental angular distributions was the one adopted (see Table III).

The HF calculation of the inelastic fluctuating contribution indicated that this process is relevant only at the two first resonance energies ($\frac{7}{2}_1^-$ and $\frac{3}{2}_1^-$). Its omission results in distortions in the fits, as will be illustrated later on. As before, these contributions are treated as a free additive parameter to the cross section obtained from the scattering matrix.

The direct amplitude was obtained by the code JUPITOR (Ref. 22) employing the parametrization defined in the analysis of the nonresonant data. Modifications were made to JUPITOR so that Coulomb excitation could be included in the 4_1^+ background amplitude. The optical phases were calculated with the code ANSPEC.[21]

The angular distributions to the 2_1^+, 4_1^+, and 2_2^+ states of ^{144}Sm were fitted at the four resonances. The analysis of the 3_1^- angular distributions was carried out only at the first resonance, since at the remaining energies the data were masked by contaminants. Besides the parameter introduced to account for the fluctuating contribution, the only free parameters still undetermined for these fits were the inelastic partial amplitudes $\Gamma_{J_\nu,c}$. Initial parameters were estimated for each of four resonances (calculation I in Sec. IV). The search for best parameters was made at each resonance, using a modified JUPITOR code. During

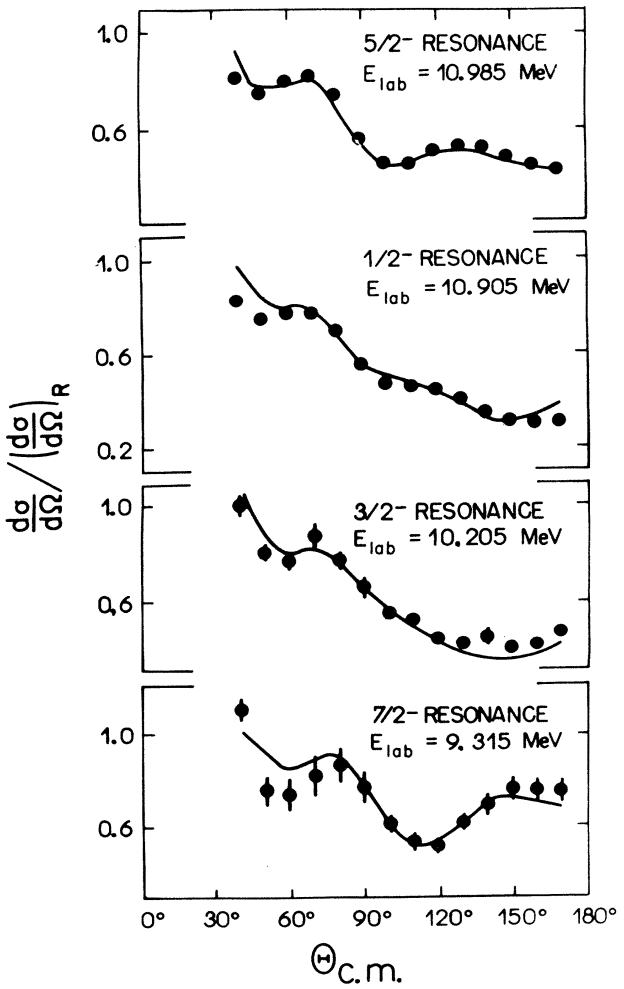

FIG. 5. Resonant elastic angular distributions. The parametrization corresponding to the fits is presented in Table III.

this procedure, for a particular resonance the parameters previously obtained for the remaining resonances were included in the calculations. Reiteration through the set of resonances was continued until the values of the parameters stabilized. The resulting values are presented in Tables IV—VII. The corresponding fits are compared to the data in Figs. 6—9. The fits are satisfactory at all the resonances, and it can be seen from these figures that the experimental data of the $\frac{7}{2}^-$ and $\frac{3}{2}^-$ resonances are frequently better reproduced by inclusion of the fluctuating cross section. In particular, the improvement of the fit obtained by considering the fluctuating contribution in the case of the 2_1^+ state at the $\frac{7}{2}_1^-$ resonance is especially remarkable. This is consoling since a major fluctuating contribution was expected in just this state.

The determination of the spectroscopic amplitudes from experimental values of $g(J_\nu,c)$ involves the calculation of single particle escape amplitudes $g^{\rm sp}(J_\nu,c)$. As was extensively discussed by Harney and Weidenmüller,[5] the different approaches for $g^{\rm sp}$ available in the literature[6–9] led to considerably different results. In the present work

TABLE IV. Partial widths for the $\frac{7}{2}^-_1$ resonance. All the widths are given in keV. The values obtained by disregarding the fluctuating contribution are indicated by (I). Those obtained by including this contribution are indicated by (II).

I_n		$\Gamma(s_{1/2},I_n)$	$\Gamma(d_{3/2},I_n)$	$\Gamma(f_{7/2},I_n)$	$\Gamma(p_{3/2},I_n)$	$\Gamma(p_{1/2},I_n)$	$\Gamma(f_{5/2},I_n)$	σ_{NC} (mb/sr)
0^+_1				7.8 ±0.8				
2^+_1	(I)			0.58 ±0.05	0.40±0.05		0.001±0.05	
	(II)			0.13 ±0.06	0.41±0.04		0.003±0.01	0.12 ±0.02
3^-_1	(I)	0.77±0.05	0.05±0.02					
	(II)	0.66±0.07	0.04±0.01					0.03 ±0.01
4^+_1	(I)			0.11 ±0.02	0.11±0.02	0.005±0.02	0.002±0.01	
	(II)			0.15 ±0.01	0.03±0.01	0.004±0.01		0.025±0.002
2^+_2	(I)			0.03 ±0.02	0.14±0.02		0.03 ±0.02	
	(II)			0.003±0.01	0.04±0.01		0.08 ±0.01	0.025±0.007

the single particle escape amplitudes were calculated using four different methods: that of Thompson, Adams, and Robson[6] (TAR); that of Zaidi, Darmodjo, and Harney[7,8] (ZDH); that of MacDonald and Mekjian[9]; and that of de Toledo Piza.[10] The results obtained with the two first methods are shown as a function of the emerging proton energy in Fig. 10. The method of de Toledo Piza gives results which are systematically about 10% greater than those obtained with the ZDH method, while the method of MacDonald and Mekjian provides g^{sp} values which are always much smaller than those obtained with the TAR method. It should be pointed out that the differences between the values furnished by the various methods are accentuated as the energy of the scattered proton increases. In other words, as the energy approaches that of the elastic scattering at the resonances of interest ($\sim$10 MeV), the discrepancies increase, and therefore the elastic amplitude $\theta(lj,I=0,J_\nu)$ turns out to be the most affected one.

Tables VIII–XI present the spectroscopic amplitudes that result from the experimental values of the inelastic partial widths (both with and without considering fluctuating contributions) and from the values of single particle escape widths obtained with the TAR and ZDH methods. In fact, considerable differences arise for $\theta(lj,0^+,J_\nu)$ as a consequence of using the approaches of TAR or ZDH. These differences become less significant as we consider increasingly excited core states.

The sum rule

$$\sum_{lj,I_n} \theta^2(lj,I_n,J_\nu) \leq 1 \tag{3.5}$$

was used as a consistency test for the analysis and for the calculations of g^{sp}. Table XII presents the values of $\sum_{lj,I_n}\theta^2$ corresponding to the results shown in Tables VIII–XI. It is observed that, when the single particle escape widths calculated with the TAR method are employed, condition (3.5) is only fulfilled for the $\frac{5}{2}^+$ state. The inclusion of the fluctuating contribution reduces the value of $\sum_{lj,I_n}\theta^2$, but the difficulty still subsists. The situation is greatly improved when the ZDH method is used; in this case the sum rule (3.5) is satisfied for all the states. It should be stressed, however, that the sum rule test cannot shed light on the necessity of including the fluctuating contribution. This may be understood by observing that the reduction of the spectroscopic amplitude for the core ground state, in general the largest one, is what allows the sum rule to be observed when employing g^{sp} values ob-

TABLE V. Partial widths for the $\frac{3}{2}^-_1$ resonance. All the widths are given in keV. The notation is the same as in Table IV.

I_n		$\Gamma(f_{7/2},I_n)$	$\Gamma(p_{3/2},I_n)$	$\Gamma(p_{1/2},I_n)$	$\Gamma(f_{5/2},I_n)$	σ_{NC} (mb/sr)
0^+_1			22 ±2			
2^+_1	(I)	2.49 ±0.2	0.41 ±0.1	0.37±0.1	0.07 ±0.1	
	(II)	2.50 ±0.04	0.21 ±0.05	0.35±0.01	0.07 ±0.1	0.027±0.007
4^+_1	(I)	0.09 ±0.02			0.003 ±0.01	
	(II)	0.07 ±0.02			0.0008±0.001	0.006±0.004
2^+_1	(I)	0.003±0.02	0.008±0.1	0.37±0.02		
	(II)	0.009±0.01	0.24 ±0.08	0.01±0.01		0.012±0.005

TABLE VI. Partial widths for the $\frac{1}{2}^-_1$ resonance. All the widths are given in keV. The notation is the same as in Table IV.

I_n	$\Gamma(f_{7/2},I_n)$	$\Gamma(p_{3/2},I_n)$	$\Gamma(p_{1/2},I_n)$	$\Gamma(f_{5/2},I_n)$
0^+_1			31.5±4	
2^+_1		1.33±0.6		3.08±0.8
4^+_1	1.38±0.4			
2^+_2		0.36±0.04		0.14±0.03

TABLE VII. Partial widths for the $\frac{5}{2}^-_1$ resonance. All the widths are given in keV. The notation is the same as in Table IV.

I_n	$\Gamma(f_{7/2},I_n)$	$\Gamma(p_{3/2},I_n)$	$\Gamma(p_{1/2},I_n)$	$\Gamma(f_{5/2},I_n)$
0^+_1				4.1±1
2^+_1	6.62±0.5	0.53 ±0.5	0.41 ±0.2	0.23±0.05
4^+_1	0.20±0.04	0.001±0.001		
2^+_2	0.06±0.02	0.16 ±0.04	0.000±0.001	

tained with the ZDH method. Thus the test loses its sensitivity to the small values of spectroscopic amplitudes associated with the core excited states, and these are the ones which are affected by the inclusion of fluctuating contributions.

We should remark that employing the g^{sp} values calculated through the method of de Toledo Piza, the sum rule is still obeyed and the resulting values of $\theta(lj,I_n,J^\pi_\nu)$ are similar to those obtained with the ZDH method.

IV. CALCULATIONS AND DISCUSSION

Theoretical spectroscopic amplitudes were obtained by describing the nucleus ^{145}Sm in the particle-vibrator model. The simpler approach of a harmonically vibrating liquid drop was first adopted for the vibrator (model I). Subsequently, the quasiparticle random phase approximation (QRPA) was employed (model II); it is supposed that the residual interaction consists of a pairing force plus a separable multipolar interaction.

A. Model I: Particle-vibrator model with a liquid drop vibrator

The Hamiltonian for the nucleus ^{145}Sm is written

$$H=H_{\rm vib}+H_{\rm sp}+H_{\rm int}\ , \tag{4.1}$$

where $H_{\rm vib}$ describes the liquid drop ^{144}Sm:

$$H_{\rm vib}=\sum_\lambda \hbar\omega_\lambda[N_\lambda+\tfrac{1}{2}(2\lambda+1)]\ , \tag{4.2}$$

with $\hbar\omega_\lambda$ and N_λ the energy and number of phonons with multipolarity λ. The single-particle Hamiltonian $H_{\rm sp}$ in the occupation representation is given by

$$H_{\rm sp}=\sum_{jm}\epsilon_j a^\dagger_{jm}a_{jm}\ , \tag{4.3}$$

where $a^\dagger_{jm}$ (a_{jm}) is the creation (annihilation) operator of a neutron in the jm orbital, j and m being, respectively, the angular momentum and its projection in the z axes; and ϵ_j are the eigenvalues of $H_{\rm sp}$. The interaction $H_{\rm int}$ between the particle and the vibrator is represented by

$$H_{\rm int}=-\sum_{\lambda=2}^{3}\left[\frac{\hbar\omega_\lambda}{2C_\lambda}\right]^{1/2}\sum_{\mu=-\lambda}^{\lambda}[b_{\lambda\mu}+(-)^{\lambda+\mu}b^\dagger_{\lambda-\mu}]\sum_{\substack{j_1m_1\\ j_2m_2}}\langle j_1m_1\,|\,i^\lambda k_\lambda(r)Y_{\lambda\mu}(\hat r)\,|\,j_2m_2\rangle a^\dagger_{j_1m_1}a_{j_2m_2}\ , \tag{4.4}$$

where C_λ is the mass parameter of the vibrator; $b^\dagger_{\lambda\mu}$ is the creation (annihilation) operator of a phonon with multipolarity λ; $|jm\rangle$ are the eigenfunctions of $H_{\rm sp}$; $k(r)$ represents the radial dependency of the interaction; and $Y_{\lambda\mu}(\hat r)$ are spherical harmonics.

The relation between C_λ and the deformation parameter β_λ introduced in the preceding section is given by

$$\beta_\lambda=\left[(2\lambda+1)\left[\frac{\hbar\omega_\lambda}{2C_\lambda}\right]\right]^{1/2}. \tag{4.5}$$

The eigenfunctions of the total Hamiltonian are obtained treating $H_{\rm int}$ as a perturbation and adopting the unperturbed basis

$$|j(N_2I_2N_3I_3)I,JM\rangle=\sum_{mM_I}(jmIM_I\,|\,JM)\,|jm\rangle\,|N_2I_2N_3I_3,IM_I\rangle\ . \tag{4.6}$$

The vector $|N_2I_2N_3I_3,IM_I\rangle$ represents the state of the vibrator with N_2 quadrupole phonons coupled to I_2, and N_3 octupole phonons coupled to I_3, where I_2 and I_3 are coupled to I. The coefficients of the expansion of the parent nucleus wave function, $|E^\nu,JM\rangle$, in this basis are just the desired spectroscopic amplitudes

$$|E^\nu,JM\rangle=\sum C_\nu(j(N_2I_2N_3I_3)I;JM)\,|j(N_2I_2N_3I_3)I,JM\rangle \tag{4.7}$$

and

$$\theta(lj,I,J_\nu)=C_\nu(j(N_2I_2,N_3I_3)I;JM)\ . \tag{4.8}$$

A calculation (calculation I) within this model was carried out by allowing for the coupled neutron six single particle orbitals: $2f_{7/2}$, $1i_{13/2}$, $3p_{3/2}$, $3p_{1/2}$, $1h_{9/2}$, and $2f_{5/2}$, whose energies are presented in Table XIII. For the radial matrix element, the estimation of Booth *et al.*[23] was adopted, viz.,

$$\langle k(r)\rangle=50\ \text{MeV}\ .$$

Core vibrational states with up to three quadrupole pho-

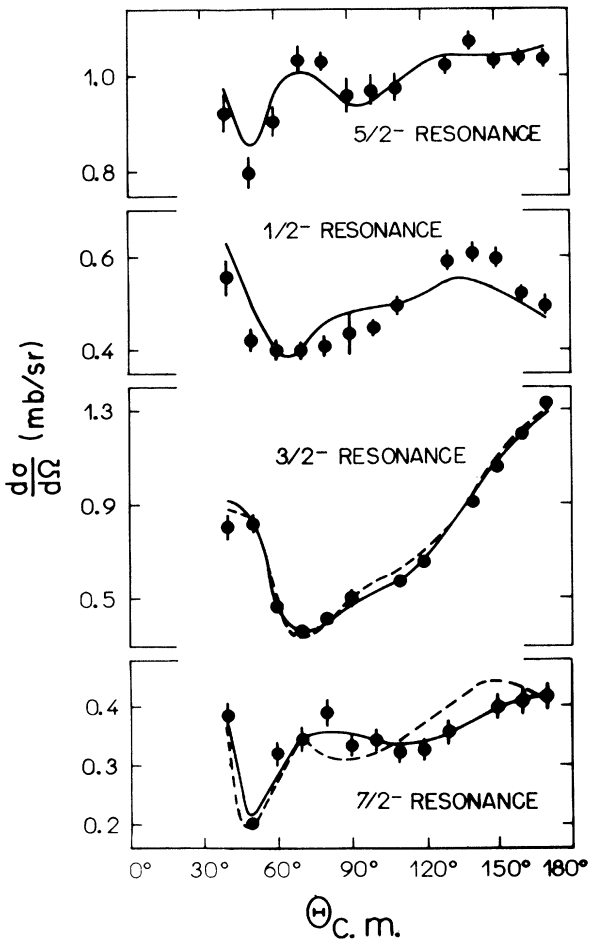

FIG. 6. Fits to the resonant angular distributions for the 2_1^+ state. For the $\frac{7}{2}_1^-$ and $\frac{3}{2}_1^-$ resonances the dashed (solid) lines correspond to the fits obtained by disregarding (considering) the fluctuating contribution.

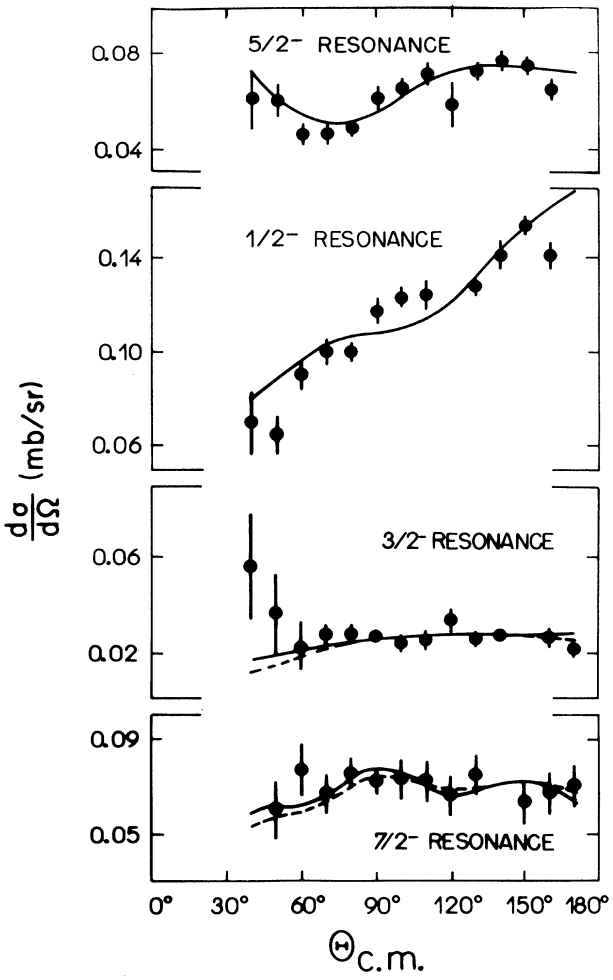

FIG. 7. Fit to the resonant angular distribution for the 3_1^- state at the $\frac{7}{2}_1^-$ resonance. The dashed (solid) lines correspond to the fit obtained by disregarding (considering) the fluctuating contribution.

nons ($N_2 \leq 3$) and up to two octupole phonons ($N_3 \leq 2$) were considered. The following experimental values of $\hbar\omega_\lambda$ and β_λ were employed (see Sec. III),

$$\hbar\omega_2 = 1.66 \text{ MeV} , \quad \hbar\omega_3 = 1.81 \text{ MeV} ,$$

$$\beta_2 = 0.070 , \quad \beta_3 = 0.108 .$$

All basis vectors with unperturbed energies smaller than 7.0 MeV were considered.

This model provides us with no information about the microscopic structure of the core (particle-hole excitations). Furthermore, it is implicitly assumed that the 4_1^+ and 2_2^+ states correspond to two quadrupole phonon excitations, which is perhaps too strong a supposition. As a consequence, the corresponding amplitudes in the parent wave functions are expected to be too small.

B. Model II: Quasiparticle random phase approximation

In this model we start with a microscopic shell model Hamiltonian,

$$H = H_{\text{sp}} + H_{\text{res}} , \tag{4.9}$$

in which the residual interaction H_{res} involves a short range component represented by the pairing force and a long range component represented by multipolar interactions. The QRPA treatment of this problem has been discussed in detail by Ruiz *et al.*,[24] and we refer the reader to this work for a detailed review and notation. Here we only describe our calculations for ^{144}Sm and ^{145}Sm nuclei.

The multipolar interaction constant χ_λ is given by the secular equation

$$\chi_\lambda^{-1} = \tfrac{1}{2} \sum_{j_1 j_2} [P(j_1 j_2 \lambda)]^2 \left[\frac{1}{E_{j_1} + E_{j_2} - \hbar\omega_{\lambda,i}} + \frac{1}{E_{j_1} + E_{j_2} + \hbar\omega_{\lambda,i}} \right] , \tag{4.10}$$

where

$$E_j=[(\epsilon_j-\epsilon_F)^2+\Delta^2]^{1/2} \tag{4.11}$$

are the independent quasiparticle energies, ϵ_F is the chemical potential, and Δ represents the energy gap. The quantity $P(j_1j_2\lambda)$ is defined as

$$P(j_1j_2\lambda)=(2\lambda+1)^{-1/2}(U_{j_1}V_{j_2}+U_{j_2}V_{j_1})\langle j_1||i^\lambda r^\lambda Y_\lambda||j_2\rangle \ , \tag{4.12}$$

where U_j and V_j are, respectively, the vacancy and occupation numbers. For a given value of χ_λ the secular equation (4.10) presents several roots $\hbar\omega_i$ (assigned by i) corresponding to the same λ and different $\Lambda_{\lambda,i}$, given by

$$\Lambda_{\lambda,i}^{-2}=\frac{\partial}{\partial(\hbar\omega_{\lambda,i})}[\chi_\lambda^{-1}]=\tfrac{1}{2}\sum_{j_1j_2}[P(j_1j_2\lambda)]^2\left[\frac{1}{(E_{j_1}+E_{j_2}+\hbar\omega_{\lambda,i})^2}-\frac{1}{(E_{j_1}+E_{j_2}-\hbar\omega_{\lambda,i})^2}\right] . \tag{4.13}$$

The QRPA formalism allows us to consider the two 2^+ core states as corresponding to two distinct one-phonon excitations (one collective, the other not) with amplitudes given by the first two roots of the secular equation. The 3_1^- and 4_1^+ states were also treated as one-phonon excitations.

Figure 11 shows the behavior of χ_λ and Λ_λ as a function of $\hbar\omega_\lambda$ for $\lambda=2$, 3, and 4. These functions were calculated with the single particle energies for protons and neutrons taken from Refs. 25–27 and listed in Table XIII. Harmonic oscillator wave functions were used in the calculation of the radial matrix elements of the interaction.

Solutions of the gap equations for the protons (open shell), with $\Delta=1.26$ MeV, obtained from binding energies,[28] simultaneously furnished the values for ϵ_F and G:

$$\epsilon_F=3.20 \text{ MeV} ,$$

$$G=0.132 \text{ MeV} .$$

The condition that the solutions of (4.10) correspond to the experimental energies of the 2_1^+, 3_1^-, and 4_1^+ states result in the values of the multipole interaction constant χ_λ presented in Table XIV. From this value of χ_2 the second root, $\hbar\omega_{2,2}=2.62$ MeV, was obtained which corresponded closely to the experimental value 2.42 MeV. Table XIV also shows the amplitudes represented by $\Lambda_{\lambda,i}^{\text{th}}$. These quantities can also be estimated from the experimental values of β_λ presented in the preceding section, through the relation

$$\Lambda_\lambda=\frac{\langle k\rangle}{\langle r^\lambda\rangle}\frac{\beta_\lambda}{(2\lambda+1)^{1/2}} . \tag{4.14}$$

Using $\langle k\rangle\simeq 50$ MeV and $\langle r^\lambda\rangle=[3/(3+\lambda)]R^\lambda$, with

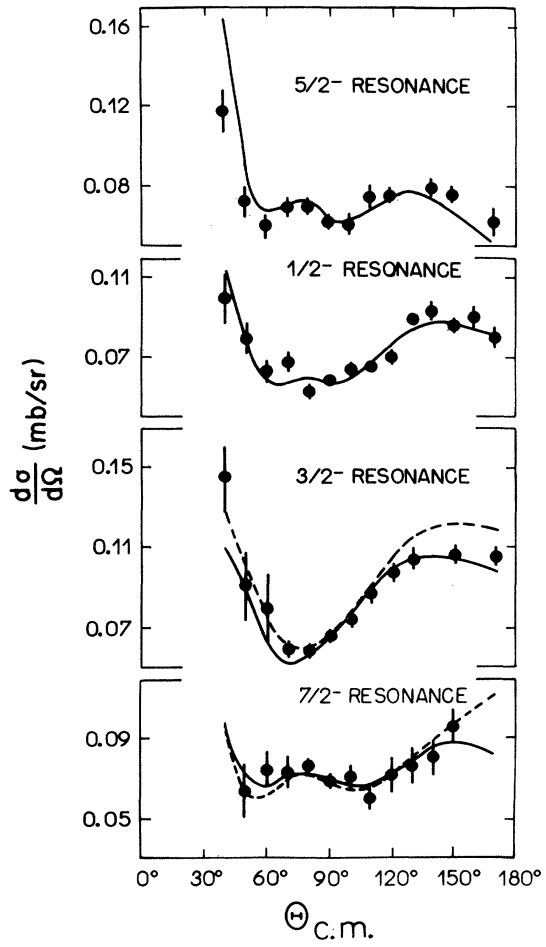

FIG. 8. Fits to the resonant angular distribution for the 4_1^+ state. For the $\frac{7}{2}_1^-$ and $\frac{3}{2}_1^-$ resonances the dashed (solid) lines correspond to the fits obtained by disregarding (considering) the fluctuating contribution.

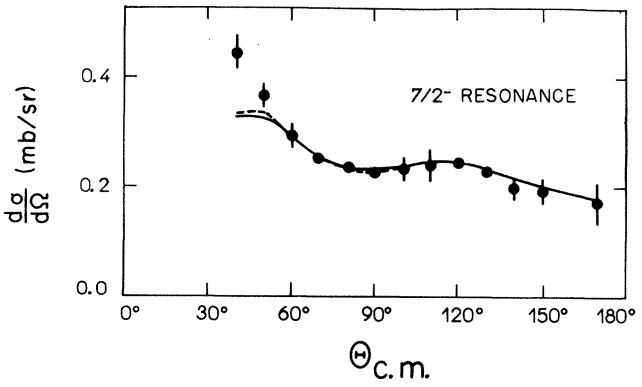

FIG. 9. Fits to the resonant angular distribution for the 2_2^+ state. For the $\frac{7}{2}_1^-$ and $\frac{3}{2}_1^-$ resonances the dashed (solid) lines correspond to the fits obtained by disregarding (considering) the fluctuating contribution.

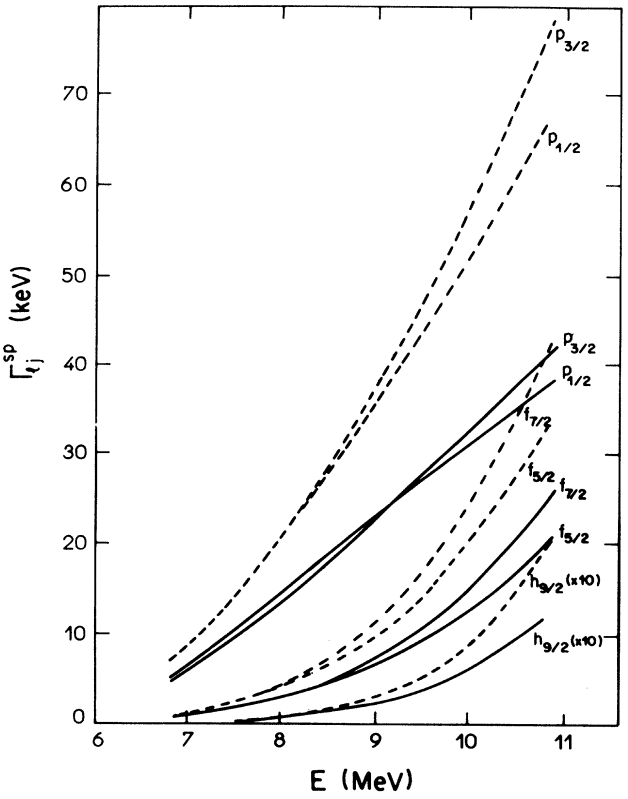

FIG. 10. Single particle escape amplitudes calculated by the methods of TAR (Ref. 6) (solid lines) and ZDH (Refs. 7 and 8) (dashed lines) as a function of the emerging proton energy.

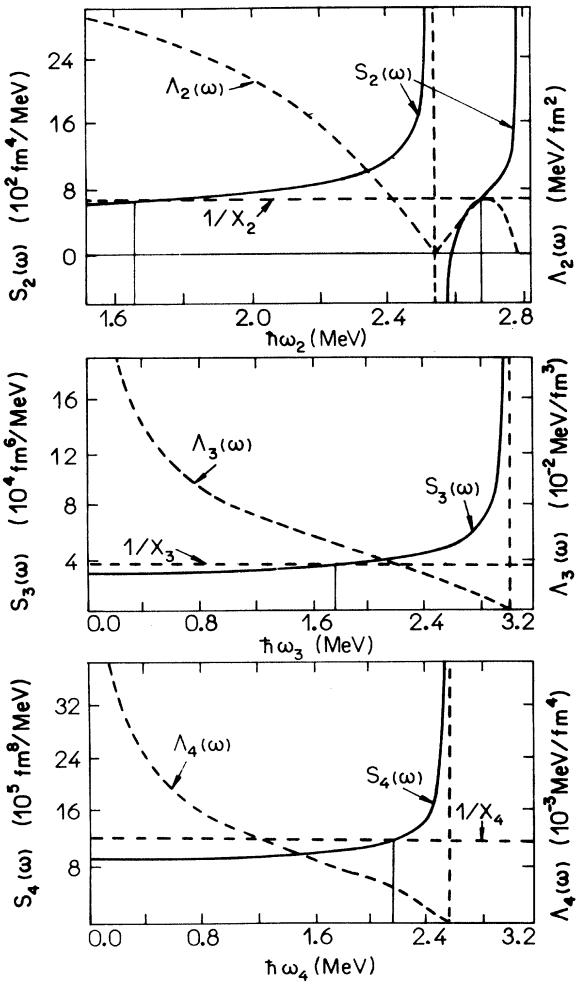

FIG. 11. Behavior of the functions $S_\lambda(\omega)$ and $\Lambda_\lambda(\omega)$ as a function of the energy $\hbar\omega_\lambda$ near the first roots of the secular equation (4.10): $\hbar\omega_2=1.66$ and 2.67 MeV, $\hbar\omega_3=1.81$ MeV, $\hbar\omega_4=2.19$ MeV. The dashed vertical lines indicate the unperturbed energies of two quasiparticles.

$r=1.2A^{1/3}$ fm (A is the mass number of the nucleus), relation (4.14) provides us with the empirical values of the amplitudes, $\Lambda_{\lambda,i}^{emp}$, listed in Table XIV. From the table we note that both estimates give similar values for Λ_3 and Λ_4. On the other hand, $\Lambda_{2,1}^{th}$ is considerably greater than $\Lambda_{2,1}^{emp}$, while $\Lambda_{2,2}^{th}$ is significantly smaller than $\Lambda_{2,2}^{emp}$. Thus one concludes that the QRPA model describes the structure of the 3_1^- and 4_1^+ states well but furnishes too much collectivity to the 2_1^+ state at the expense of the 2_2^+ state. To account for this effect we employed the empirical values of $\Lambda_{2,1}$ and $\Lambda_{2,2}$. Moreover, up to two quadrupole phonons of the first kind were considered, while for the other vibrational fields only one phonon state was taken into account. The results obtained within this framework will be labeled calculation II.

Another calculation (calculation III) was performed within the QRPA model using the same configuration space and the same parametrization as in the preceding case, except that here we have employed the empirical values of the energies $\hbar\omega_\lambda$ and of the coupling constants Λ_λ. Furthermore, in this case we used the estimate $\langle k\rangle=50$ MeV. In both QRPA calculations the spectroscopic amplitudes were evaluated by means of Eq. (4.23) of Ref. 24.

Figure 12 compares the ^{145}Sm spectrum obtained from the above-mentioned calculations with the experimental one.[4] It is observed that the low energy spectrum is always well reproduced, with the exception of the $\frac{1}{2}_1^-$ state, which lies too low in energy with the two latter calculations. The better agreement with the experimental data achieved with the first calculation is ascribed to the utilization of single-particle energies of Heyde *et al.*,[26] which were obtained by fitting the low energy spectrum within model I.

The calculated spectroscopic amplitudes are presented in Tables VIII–XI, where they can be compared to their experimental values. All three calculations provided similar values for the spectroscopic amplitudes associated with elastic scattering $\theta(lj,0^+,J_\nu^\pi)$ and, in general, a reasonable agreement with the experimental values was obtained.

The amplitudes associated with the 2_1^+ state, $\theta(lj,2_1^+,J_\nu^\pi)$, resulting from different calculations are quite similar, a reflection of the equivalency among the corresponding model descriptions. For $J_\nu^\pi=\frac{3}{2}_1^-$, $\frac{1}{2}_1^-$, and $\frac{5}{2}_1^-$ levels a satisfactory agreement between theoretical and ex-

TABLE VIII. Spectroscopic amplitudes for the $\frac{7}{2}^-_1$ state of ^{145}Sm. The results obtained from the fits that disregard (consider) the fluctuating contribution are indicated by TAR (TARCN) when the single particle escape widths are evaluated with the TAR method (Ref. 6) and by ZDH (ZDHCN) when they are calculated with the ZDH method (Refs. 7 and 8). We have indicated by CI, CII, and CIII the model calculations I, II, and III, respectively.

	I_n	$\theta(p_{1/2},I_n,\frac{7}{2}^-_1)$	$\theta(d_{3/2},I_n,\frac{7}{2}^-_1)$	$\theta(f_{7/2},I_n,\frac{7}{2}^-_1)$	$\theta(p_{3/2},I_n,\frac{7}{2}^-_1)$	$\theta(p_{1/2},I_n,\frac{7}{2}^-_1)$	$\theta(f_{5/2},I_n,\frac{7}{2}^-_1)$
TAR				0.94±0.10			
ZDH				0.75±0.08			
CI	0^+_1			0.91			
CII				0.85			
CIII				0.90			
TAR				−0.59±0.05	−0.20±0.03		0.03±0.2
ZDH				−0.48±0.04	−0.16±0.02		0.02±0.2
TARCN				−0.28±0.06	−0.20±0.02		0.05±0.2
ZDHCN	2^+_1			−0.23±0.05	−0.17±0.02		0.04±0.1
CI				−0.26	−0.15		−0.04
CII				−0.26	−0.14		−0.04
CIII				−0.25	−0.14		−0.04
TAR		−0.20±0.02	−0.09±0.04				
ZDH		−0.17±0.01	−0.08±0.03				
TARCN		−0.18±0.02	−0.09±0.02				
ZDHCN	3^-_1	−0.16±0.02	−0.08±0.02				
CI							
CII		−0.18	−0.11				
CIII		−0.19	−0.12				
TAR				0.36±0.06	0.13±0.02	0.03±0.1	0.04±0.2
ZDH				0.30±0.05	0.11±0.02	0.02±0.1	0.04±0.2
TARCN				0.43±0.03	0.07±0.02	0.03±0.06	
ZDHCN	4^+_1			0.35±0.02	0.05±0.02	0.02±0.06	
CI				0.04	0.02	0.02	0.01
CII				0.16	0.10	0.11	0.07
CIII				0.08	0.05	0.05	0.03
TAR				0.21±0.1	−0.17±0.03		0.24±0.1
ZDH				0.17±0.1	−0.14±0.03		0.20±0.1
TARCN				−0.02±0.08	−0.09±0.02		0.38±0.1
ZDHCN	2^+_2			−0.02±0.06	−0.07±0.02		0.32±0.1
CI				0.003	−0.04		0.008
CII				−0.08	−0.06		0.02
CIII				−0.09	−0.06		0.02

perimental results is obtained. One should note, however, that although an agreement is observed within the experimental errors for the $\frac{1}{2}^-_1$ state, the theory predicts in this case a major contribution of the component with $lj=p_{3/2}$ relative to the $f_{7/2}$ component, while the experimental results show an inverse behavior. In the case of the $\frac{7}{2}^-_1$ state the theoretical and experimental values of $\theta(f_{7/2},2^+_1,\frac{7}{2}^-_1)$ disagree significantly with each other when the fluctuating contribution is neglected. Inclusion of this process affects mostly only the foregoing amplitude, reducing it to half of its previous value. The resulting agreement then achieved between theoretical and experimental values is quite satisfactory.

Within model I it is not possible to account for the inelastic scattering to the 3^-_1 state. On the other hand, calculations II and III, performed within the QRPA framework, give rise to quite similar results for the theoretical amplitudes $\theta(s_{1/2},3^-_1,\frac{7}{2}^-_1)$ and $\theta(d_{3/2},3^-_1,\frac{7}{2}^-_1)$, which agree with the experimental data.

The description of the 4^+_1 state is different in each calculation. As was expected, calculation I provides amplitudes which are too small, especially for the $\frac{7}{2}^-_1$ and $\frac{3}{2}^-_1$

TABLE IX. Spectroscopic amplitudes for the $\frac{3}{2}_1^-$ state of ^{145}Sm. The notation is the same as in Table VIII.

	I_n	$\theta(f_{7/2}, I_n, \frac{3}{2}_1^-)$	$\theta(p_{3/2}, I_n, \frac{3}{2}_1^-)$	$\theta(p_{1/2}, I_n, \frac{3}{2}_1^-)$	$\theta(f_{5/2}, I_n, \frac{3}{2}_1^-)$
TAR			0.81 ±0.07		
ZDH			0.61 ±0.05		
CI	0_1^+		0.71		
CII			0.67		
CIII			0.70		
TAR		−0.75 ±0.06	−0.15 ±0.04	−0.14±0.04	−0.13±0.2
ZDH		−0.60 ±0.05	−0.12 ±0.03	−0.12±0.03	−0.11±0.2
TARCN		−0.75 ±0.01	−0.11 ±0.03	−0.14±0.01	−0.13±0.2
ZDHCN	2_1^+	−0.61 ±0.01	−0.09 ±0.02	−0.11±0.01	−0.11±0.2
CI		−0.61	−0.18	−0.13	−0.08
CII		−0.55	−0.17	−0.15	−0.07
CIII		−0.59	−0.17	−0.13	−0.08
TAR		0.19 ±0.04			0.04±0.1
ZDH		0.16 ±0.04			0.03±0.1
TARCN		0.17 ±0.05			0.02±0.02
ZDHCN	4_1^+	0.14 ±0.04			0.02±0.02
CI		0.08			0.04
CII		0.23			0.16
CIII		0.12			0.08
TAR		−0.04 ±0.2	0.005±0.06	−0.18±0.01	
ZDH		−0.03 ±0.2	0.004±0.05	−0.15±0.01	
TARCN		−0.067±0.07	−0.15±0.02	−0.04±0.03	
ZDHCN	2_2^+	−0.055±0.06	−0.12 ±0.02	−0.03±0.02	
CI		0.14	0.05	0.03	
CII		−0.13	−0.06	−0.06	
CIII		−0.16	−0.06	−0.05	

TABLE X. Spectroscopic amplitudes for the $\frac{1}{2}_1^-$ state of ^{145}Sm. The notation is the same as in Table VIII.

	I_n	$\theta(f_{7/2}, I_n, \frac{1}{2}_1^-)$	$\theta(p_{3/2}, I_n, \frac{1}{2}_1^-)$	$\theta(p_{1/2}, I_n, \frac{1}{2}_1^-)$	$\theta(f_{5/2}, I_n, \frac{1}{2}_1^-)$
TAR				0.91±0.12	
ZDH				0.68±0.09	
CI	0_1^+			0.78	
CII				0.73	
CIII				0.77	
TAR			0.23±0.10		−0.64±0.02
ZDH			0.18±0.08		−0.52±0.1
CI	2_1^+		0.47		−0.29
CII			0.30		−0.23
CIII			0.35		−0.26
TAR		−0.26±0.08			
ZDH		−0.21±0.08			

TABLE X. (*Continued*).

	I_n	$\theta(f_{7/2},I_n,\frac{1}{2}_1^-)$	$\theta(p_{3/2},I_n,\frac{1}{2}_1^-)$	$\theta(p_{1/2},I_n,\frac{1}{2}_1^-)$	$\theta(f_{5/2},I_n,\frac{1}{2}_1^-)$
CI	4_1^+	−0.24			
CII		−0.46			
CIII		−0.32			
TAR			0.14±0.02		−0.19±0.04
ZDH			0.11±0.01		−0.16±0.03
CI	2_2^+		−0.11		0.06
CII			0.10		−0.08
CIII			0.12		−0.10

states. In addition, not one of the calculations was able to reproduce the signs of the spectroscopic amplitudes for the $\frac{5}{2}_1^-$ state, and calculation II systematically furnishes amplitudes which are twice as large as those of calculation III. It is this latter calculation which best agrees with experiments. The $\theta(p_{3/2},4_1^+,\frac{7}{2}_1^-)$ amplitude agrees with calculation I when the fluctuating contribution is neglected. But, when this effect is included, the "experimental value" of the foregoing amplitude is reduced by a factor of 2, thus falling into agreement with calculation III.

The 2_2^+ state is very badly described within model I, since the theoretical amplitudes turn out to be, in most cases, too small and have the wrong signs in comparison with the experimental values. It should be stressed that inclusion of the fluctuating contribution for the core state is essential for getting an agreement between experimental and theoretical values. The amplitudes which are mostly affected (producing even the necessary changes in the signs) are $\theta(f_{7/2},2_2^+,\frac{7}{2}_1^-)$ and $\theta(p_{3/2},2_2^+,\frac{3}{2}_1^-)$. The inclusion of the fluctuating process is also responsible for the reduction of the $\theta(f_{7/2},2_2^+,\frac{3}{2}_1^-)$ and $\theta(p_{1/2},2_2^+,\frac{3}{2}_1^-)$ amplitudes and the increase of the $\theta(f_{7/2},2_2^+,\frac{3}{2}_1^-)$ ampli-

TABLE XI. Spectroscopic amplitudes for the $\frac{5}{2}_1^-$ state of ^{145}Sm. The notation is the same as in Table VIII.

	I_n	$\theta(f_{7/2},I_n,\frac{5}{2}_1^-)$	$\theta(p_{3/2},I_n,\frac{5}{2}_1^-)$	$\theta(p_{1/2},I_n,\frac{5}{2}_4^-)$	$\theta(f_{5/2},I_n,\frac{5}{2}_1^-)$
TAR					0.44±0.11
ZDH					0.35±0.09
CI	0_1^+				0.37
CII					0.50
CIII					0.45
TAR		0.87±0.19	0.15 ±0.1	−0.13 ±0.06	−0.17±0.04
ZDH		0.69±0.15	0.11 ±0.1	−0.10 ±0.04	−0.14±0.03
CI	2_1^+	0.83	0.12	−0.11	−0.10
CII		0.66	0.12	−0.18	−0.13
CIII		0.76	0.11	−0.14	−0.11
TAR		0.19±0.04	0.006±0.01		
ZDH		0.08±0.02	0.005±0.01		
CI	4_1^+	−0.15	−0.06		
CII		−0.17	−0.18		
CIII		−0.09	−0.08		
TAR		0.11±0.04	−0.09 ±0.02	0.001±0.04	
ZDH		0.09±0.03	−0.08 ±0.02	0.001±0.03	
CI	2_2^+	−0.07	−0.12	0.03	
CII		0.03	0.03	−0.05	
CIII		0.03	0.03	−0.05	

TABLE XII. The $\sum_{lj,I_n}\theta^2(lj,I_n,J)$ for each studied state. The notation is the same as in Table VIII.

	J_ν^π			
	$\frac{7}{2}^-_1$	$\frac{3}{2}^-_1$	$\frac{1}{2}^-_1$	$\frac{5}{2}^-_1$
TAR	1.60±0.36	1.35±0.33	1.41±0.30	1.08±0.20
ZDH	1.05±0.35	0.82±0.32	0.85±0.20	0.66±0.07
TARCN	1.39±0.27	1.32±0.24		
ZDHCN	0.91±0.20	0.81±0.22		

tude, producing in this way good agreement between theoretical predictions and experimental values. Finally, for the $\frac{1}{2}^-_1$ state we observe that the theoretical amplitudes $\theta(lj,2_2^+,\frac{1}{2}^-_1)$ are close to the experimental values, while for the $\frac{5}{2}^-_1$ state none of the calculations was able to correctly reproduce the signs of the experimental amplitudes.

V. CONCLUSION

From an analysis of proton angular distributions at four isobaric analog resonances of the ^{144}Sm+p system we have extracted spectroscopic information about the corresponding low-lying states of the ^{145}Sm nucleus. Among these results only those relative to the 0_1^+ and 2_1^+ core states have been available in the literature,[1–4] and even these presented inconsistencies which were attributed to the adopted description of the background.[4] The data reported by Martin *et al.*[3] suggested to us that configurations involving the 3_1^-, 4_1^+, and 2_2^+ states of ^{144}Sm should be relevant in building up the parent state wave functions, and this was confirmed by the corresponding spectroscopic information that was obtained for the first time in the present work.

TABLE XIII. Single particle energies for neutrons and protons. The gaps between the shells were obtained from the differences $Q_{\gamma n}-Q_{n\gamma}$ or $Q_{\gamma p}-Q_{p\gamma}$ for the corresponding closed shell nuclei [Q_{xy} represents the threshold for the (x,y) reaction.] The values of ϵ_{nlj} were taken from Refs. 25–27.

nlj	ϵ^{sp}_{nlj} (neutrons) (MeV)	ϵ^{sp}_{nlj} (protons) (MeV)
$2f_{5/2}$	2.25	8.94
$3p_{1/2}$	1.80	10.77
$3p_{3/2}$	1.21	9.49
$1h_{9/2}$	1.35	5.92
$1i_{13/2}$	1.50	8.30
$2f_{7/2}$	0.00	6.30
$2d_{3/2}$	−3.79	1.70
$3s_{1/2}$	−4.20	1.45
$1h_{11/2}$	−4.94	1.30
$2d_{5/2}$	−5.15	0.00
$1g_{7/2}$	−5.94	−0.70
$1g_{9/2}$	−10.56	−5.48
$2p_{1/2}$	−11.28	−5.58
$2p_{3/2}$	−12.57	−7.48
$1f_{5/2}$	−12.76	−7.98
$1f_{7/2}$	−15.75	−10.96

An appreciable effort was invested in order to obtain a precise description of the background. The direct scattering was treated within the coupled channel approach, which was preferable to the usual DWBA representation. The fluctuating contribution was also taken into account, and proved to be relevant at the first two resonances, especially for the scattering to the 2_1^+ and 2_2^+ states of ^{144}Sm.

The magnitudes of the spectroscopic amplitudes extracted from the experimental data depend, in addition, on the method employed in the estimate of the single-particle escape amplitudes. The analysis performed here suggests that the method of Zaidi, Damodjo, and Harney[7,8] and that of de Toledo Piza[10] could be more realistic than that of Thompson, Adams, and Robson[6] and of Mac Donald and Mekjian.[9]

The experimental spectroscopic amplitudes were compared to calculations based on the particle-vibrator model, with the vibrator approximated at first by a liquid drop, and then treated within the QRPA. With the last representation good agreement was always observed, while for

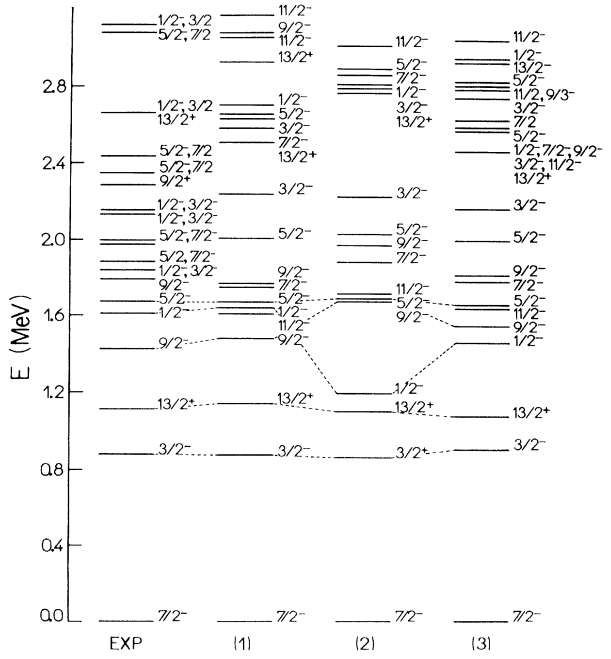

FIG. 12. Experimental (Ref. 4) and calculated energy levels of ^{145}Sm. The spectra indicated by (1), (2), and (3) were obtained by calculations I, II, and III, respectively.

TABLE XIV. Calculated values of the coupling constants χ_λ and theoretical and empirical values for the particle-phonon vertix amplitudes Λ_λ.

λ	i	$\hbar\omega_{\lambda,i}$ (MeV)	$\chi_{\lambda,i}$ (MeV/fm$^{2\lambda}$)	$\Lambda^{th}_{\lambda,i}$ (MeV/fm$^{\lambda}$)	$\Lambda^{emp}_{\lambda,i}$ (MeV/fm$^{\lambda}$)
2	1	1.66	1.45×10^{-3}	0.074	0.053
3	1	1.81	2.94×10^{-5}	0.012	0.014
4	1	2.19	0.80×10^{-6}	0.0012	0.0011
2	2	2.67	1.45×10^{-3}	0.015	0.030

the liquid drop vibrator this did not occur, especially for the 3^-_1 and 2^+_2 core states. This showed the importance of considering the microscopic structure of the core. The agreement observed between the experimental and theoretical spectroscopic amplitudes when the fluctuating contribution is taken into account is quite impressive, pointing out the necessity of including this contribution in the description of the background for the ^{144}Sm+p system and giving credence to our procedure. It would be of interest to independently calculate the fluctuation contributions to the cross sections and so avoid the uncertainties arising from adjusting their values. However, rigorous calculations require level information not presently available, and pose theoretical difficulties because of interaction between the analog resonances and the $T^<$ state responsible for the fluctuation cross section.

ACKNOWLEDGMENTS

We are deeply grateful to Elizabeth Farrelly Pessoa for a very careful reading of the manuscript and for very useful discussions. One of us, J. L. Foster, would like to thank the IPN, Orsay France and J. P. Schapira for their hospitality during a two month stay. IPN supplied the computer time for the preliminary reaction analysis. One of us (F.K.) is pleased to acknowledge many extremely helpful discussions with A. F. R. de Toledo Piza. F.K. is a member of the Carrera de Investigador Científico, Consejo Nacional de Investigación Cientifica y Tecnológica, Argentina and was sponsored by Financiadora de Estudos e Projetos, Brasil.

*Permanent address: Departamento de Física, Facultad de Ciencias Exactas, Universidad Nacional de La Plata, 1900 La Plata, Argentina.

[1]K. Marouchian, P. von Brentano, J. P. Wurm, and S. A. A. Zaidi, Z. Naturforsch. Teil A 21, 929 (1966).
[2]R. K. Jolly and C. F. Moore, Phys. Rev. 155, 1377 (1967).
[3]R. Martin, L. Bimbot, S. Gales, L. Lessard, D. Spalding, W. G. Weitkamp, O. Dietzsch, and J. L. Foster, Jr., Nucl. Phys. A210, 221 (1973).
[4]H. Clement, G. Graw, R. Zenger, and G. Zöllner, Nucl. Phys. A285, 109 (1977).
[5]H. L. Harney and H. A. Weidenmüller, Nucl. Phys. A139, 241 (1969).
[6]W. J. Thompson, J. L. Adams, and D. Robson, Phys. Rev. 173, 975 (1968).
[7]S. A. A. Zaidi and S. Darmodjo, Phys. Rev. Lett. 19, 1446 (1967).
[8]H. L. Harney, Nucl. Phys. A119, 591 (1968).
[9]A. Mekjian and W. M. Mac Donald, Nucl. Phys. A121, 385 (1968).
[10]A. F. R. de Toledo Piza, Instituto de Física, Universidade de São Paulo, Brazil, Technical Report TABU, 1971 (unpublished).
[11]F. G. Perey, Phys. Rev. 132, 755 (1963).
[12]J. Raynal, Centre d'Études Nucleaires, Saclay, France, Technical Report MAGADI, 1969 (unpublished).
[13]J. H. Barker and J. C. Hiebert, Phys. Rev. C 4, 2256 (1971).
[14]P. B. Woollan, R. J. Griffiths, and N. M. Clarke, Nucl. Phys. A189, 321 (1972).
[15]P. B. Woollan, R. J. Griffiths, J. L. Parish, J. G. Kulleck, R. F. Moore, and P. von Brentano, Phys. Rev. 165, 1312 (1968).
[16]D. Larson, S. M. Austin, and B. H. Wildenthal, Phys. Rev. 175, 1482 (1968).
[17]J. Raynal, code ECIS, Centre d'Études Nucleaires, Saclay, France, 1969 (unpublished).
[18]E. Sheldon and V. C. Rogers, Comput. Phys. Commun. 6, 99 (1973).
[19]A. Gilbert and A. G. W. Cameron, Can. J. Phys. 43, 1446 (1965).
[20]F. D. Becchetti, Jr. and G. W. Greenlees, Phys. Rev. 182, 1190 (1969).
[21]W. J. Thompson and J. L. Adams, Tandem Accelerator Laboratory, Florida State University, Tallahassee, Technical Report ANSPEC, 1967 (unpublished).
[22]T. Tamura, Rev. Mod. Phys. 37, 679 (1965).
[23]W. Booth, S. Wilson, and S. S. Ipson, Nucl. Phys. A229, 61 (1974).
[24]M. C. Hermida, M. Ruiz, M. L. Cescato, J. L. Foster, Jr., and F. Krmpotić, Phys. Rev. C 29, 64 (1984), the following paper.
[25]H. Heyde, W. Warouquier, and H. Vincx, Phys. Lett. 57B, 429 (1975).
[26]B. H. Wildenthal, E. Newman, and R. L. Auble, Phys. Rev. 82, 690 (1971).
[27]A. Covello, V. R. Manfredi, and N. Azziz, Nucl. Phys. A201, 215 (1973).
[28]A. Bohr and B. R. Mottelson, *Nuclear Structure* (Benjamin, New York, 1969), Vol. I.